ACS Photonics

Article

pubs.acs.org/journal/apchd5

Multiphoton Photoemission Microscopy of High-Order Plasmonic Resonances at the Ag/Vacuum and Ag/Si Interfaces of Epitaxial Silver Nanowires

Maciej Dąbrowski, Yanan Dai, Adam Argondizzo, Qiang Zou, Xuefeng Cui, and Hrvoje Petek*

Department of Physics and Astronomy and Pittsburgh Quantum Institute, University of Pittsburgh, Pittsburgh, Pennsylvania 15260, United States

ABSTRACT: Understanding the physics of surface plasmons and related phenomena requires knowledge of the spatial, temporal, and spectral distributions of the total electromagnetic field excited within nanostructures and their interfaces, which reflects the electromagnetic mode excitation, confinement, propagation, and damping. We present a microscopic and spectroscopic study of the plasmonic response in single-crystalline Ag wires grown *in situ* on Si(001) substrates. Excitation of the plasmonic modes with broadly tunable (UV−IR) femtosecond laser pulses excites ultrafast multiphoton photoemission, whose spatial distribution is imaged with an aberration-corrected photoemission electron microscope, thereby providing a time-integrated map of the locally enhanced electromagnetic fields. We show by tuning the wavelength, polarization, and *k*-vector of the incident laser light that for a few micrometers long wires we can selectively excite either the propagating surface plasmon polariton modes or high-order multipolar resonances of the Ag/vacuum and Ag/Si interfaces. Moreover, upon tuning the excitation wavelength from the UV to the near-IR spectral regions, we find that the resonant plasmonic modes shift from the top of the wires to selvedge at the Ag/Si interface. Our results, supported by numerical simulations, provide a better understanding of the optical response of metal/semiconductor structures and guidance toward the design of polaritonic and nanophotonic devices with enhanced properties, as well as suggest mechanisms for plasmonically enhanced photocatalysis.

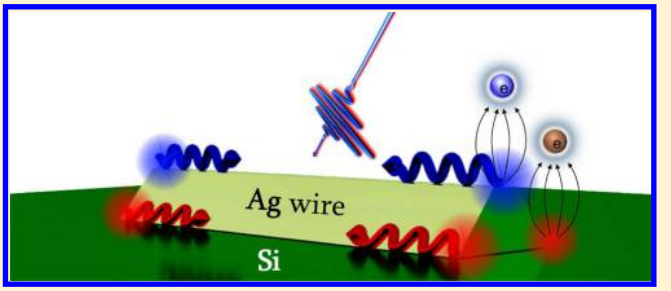

KEYWORDS: *PEEM, high-order plasmon, nanowire, Ag/Si plasmon, ultrafast microscopy*

Coupled quasiparticles of photons and charge-density fluctuations, known as surface plasmon polaritons (SPPs), have the potential to impact the next generation of information-processing devices by combining electronics and optics at the nanometer scale.[1,2] Among the variety of different materials and structures being studied, crystalline Ag nanowires are particularly germane because they support sharp plasmonic modes in the IR to UV spectral regions and can simultaneously act as plasmonic nanoantennas,[3−5] resonators,[6−9] waveguides,[10−12] etc. Moreover, there is tremendous interest in metal−semiconductor nanocomposites, which can support hybrid plasmonic−excitonic modes and have the potential to enhance solar energy conversion, for example, through hot electron transfer,[13] enhanced light scattering,[14] and plasmon−exciton dipole coupling.[15−18]

Numerous studies have been performed to demonstrate and characterize the above phenomena in metallic nanowires.[6−8,19,20] When studying plasmonic properties, the focus has been either on subwavelength structures, with size features much smaller than the excitation wavelength where strong localization is observed and the system can be described within quasistatic limit, or on structures comparable in size to the wavelength, where in addition propagating plasmons can be observed but retardation effects must also be included for a theoretical description of the localized fields.[21] Such division of emphasis partially stems from the experimental limitations since it is difficult to obtain a single system with varying structures sustaining both propagating and localized plasmons, as well as to image their properties on multiple length scales. A large number of parameters strongly affecting the plasmonic properties such as shape and size, dielectric properties of the medium and environment, and the type of excitation, cause the results to be often assigned to particular systems. Furthermore, experiments tend to focus on the optically brightest dipole modes, but in many systems higher order modes can be excited to reveal rich physics of light−metal and metal−semiconductor interactions, which require sophisticated spectroscopic and microscopic techniques to illuminate.

A further challenge is to image plasmonic phenomena on their natural temporal and spatial scales.[22,23] Various ingenious techniques have been developed to image ultrafast processes on the nanometer scale.[24,25] Conventional optical methods have fast time resolution but are limited in spatial resolution, according to the Abbe criterion, to approximately half the wavelength of light. Scanning near-field optical microscopy is

Received: May 22, 2016

DOI: 10.1021/acsphotonics.6b00353
ACS Photonics XXXX, XXX, XXX−XXX

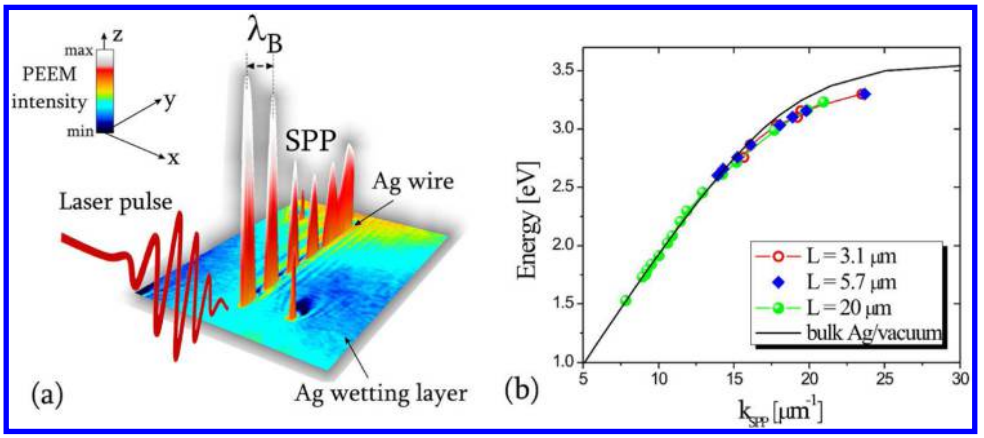

Figure 1. (a) Schematic of an SPP excitation and observation in a PEEM experiment. The laser pulse excites an SPP propagating on top of a Ag wire and interferes with it, forming the beating pattern with a period λ_B. The 3D PEEM image is acquired for a 20 μm long Ag wire upon longitudinal excitation with TM polarized light with a photon energy of 2.6 eV. (b) Dispersion relation for Ag wires of different lengths L. The experimental data are compared to the dispersion relation for the bulk Ag/vacuum interface, using the dielectric constants from ref 42.

capable of both high spatial and temporal resolution, but suffers from a low-throughput serial data acquisition.[23] Electron beam based methods offer high spatial resolution in electron energy loss and cathodoluminescence modes, but have difficulty achieving few femtosecond temporal resolution.[26,27] By employing ultrafast optical excitation and photoelectron imaging capabilities time-resolved photoemission electron microscopy (TR-PEEM) uniquely combines the requisite temporal and spatial resolution with highly parallel data acquisition, making it ideally suited for studying dynamical plasmonic phenomena on the nanofemto scale.[22,28] By combining TR-PEEM with a broadly tunable femtosecond laser source we demonstrate its capability for spectroscopic and microscopic studies of plasmonic nanostructures.

Specifically, we present a real-space TR-PEEM observation of propagating and localized plasmons in epitaxially grown single-crystalline Ag nanowires on a Si(001) substrate.[20,29] The broadly tunable ultrafast laser excitation reveals a wide range of uniquely defined resonances within *in situ* grown Ag/Si(001) structures. The plasmonic modes are imaged by nonlinear photoelectron emission whereby intense plasmonic fields drive multiphoton excitation of electrons above the local vacuum level [expected to be 4.6 eV[30] above the Fermi level for the exposed Ag(001) facets of the nanowires].[22,31] Photoelectrons produced through the multiphoton photoemission (mPP) process are imaged with the high spatial resolution (<10 nm) PEEM. Different plasmonic modes are selectively excited, and their spatial distributions revealed by recording mPP-PEEM images for varying wavelengths, polarizations, and k-vectors of the excitation light. In contrast to previous reports,[6−8,32,33] where the longitudinal multipolar modes along the major axis of nanowires have been observed, we mainly study the transverse surface plasmon modes driven by the incident laser light with the k-vector perpendicular to the major axis of the wire for which the excitation mechanisms are less well established. In particular we focus on the low-energy surface plasmons that are localized at the Ag/Si interface and thereby involve strong metal−semiconductor coupling. We show that these modes possess antisymmetric character of the electric field component perpendicular to the surface and are bound to the junction of the Si−Ag−vacuum media where the trapezoidal Ag wires converge to an atomically sharp apex.

EXPERIMENTAL DETAILS

All the experiments are performed within the aberration-corrected low-energy electron microscope/photoemission electron microscope (AC-LEEM/PEEM) instrument (SPECS)[34] with a base pressure of 2×10^{-10} mbar. A clean Si(001) surface with (2×1) reconstruction is prepared by repeated heating of the sample to ∼1500 K. The Si surface quality is confirmed by LEEM imaging in a dark field mode, which shows the contrast from alternating 2×1 domains with orthogonally propagating dimer rows on terraces that differ by single atomic layer height.[35] Deposition of Ag at elevated temperature T = 800 K leads to a Stranski−Krastanov growth mode consisting of a Ag-(2×3) wetting layer that is in equilibrium with Ag pyramids and wires, which grow to submicrometer height and width dimensions.[36,37] The focus here is on Ag nanowires, which can be grown to ∼20 μm lengths before the plasmonic excitations of nearby nanostructures begin interfering with the imaging of the nanowire modes. Several samples are grown to obtain a range of structures for the reported data and confirm reproducibility.

The excitation source for mPP measurements is a dual noncollinear optical parametric amplifier (NOPA) source pumped by the second and third harmonics of an Yb-doped fiber laser (Clark-MXR Impulse). The pump laser operates at 1035 nm with a variable pulse repetition rate from 0.2 to 2 MHz, 10 μJ per pulse energy, and ∼250 fs pulse duration. A portion of the output is focused into a sapphire plate to generate a white light continuum, which serves as a seed pulse for the NOPA. The second and third harmonics of the pump laser amplify portions of the white continuum to generate tunable pulses in the 680−900 and 500−650 nm (1.82−1.38 and 2.48−1.91 eV) bands. Frequency doubling of the NOPA light in a β-$BaBO_3$ (BBO) crystal produces tunable excitation pulses in the 270−420 nm (4.6−2.9 eV) band. Dispersion compensation by matched pairs of negative dispersion mirrors delivers typically ∼30 fs duration pulses to the sample. The excitation light incident at 70° with respect to the surface normal irradiates a 50×100 μm spot at the focal plane of the LEEM/PEEM electron imaging optics. The laser polarization with respect to the optical plane is adjusted with a $\lambda/2$ plate.

The total field present in the sample, combining the amplitudes of the external field with those of the scattered fields and excited plasmonic modes, drives the nonlinear

DOI: 10.1021/acsphotonics.6b00353
ACS Photonics XXXX, XXX, XXX−XXX

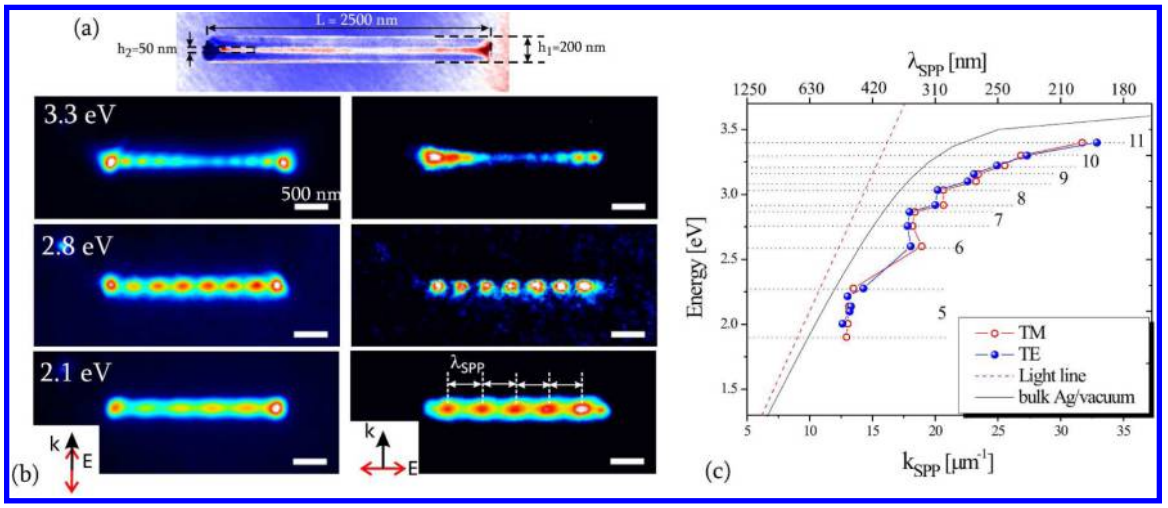

Figure 2. (a) Geometric characterization of a Ag nanowire by LEEM in the mirror mode (incident electron energy close to zero) for a Ag wire with dimensions: h_1 = 200, h_2 = 50, and L = 2500 nm. (b) PEEM images of the Ag wire (a) upon excitation with different wavelengths and for two polarizations: TM (left column) and TE (right column). (c) Dispersion relation of the TM and TE in-plane k_{SPP} extracted from the PEEM images such as shown in (b). The number of antinodes (nodes) for the TM (TE) mode is shown, and their energy span is marked by dashed horizontal lines. For reference, the light line and bulk Ag/vacuum dispersion curves are shown.

photoemission corresponding to absorption of two, three, or four photons (2PP, 3PP, and 4PP processes), as necessary to overcome the sample work function. Due to the plasmonic field enhancement, mPP emission maps the local density of states of the dominantly excited plasmonic modes through interference between the external and plasmonic fields. The photoemitted electrons are collected and their spatial distributions are imaged with the AC-PEEM optics to generate maps of the local field enhancements and interferences generated by the nanostructured sample.[38] In addition, 1PP PEEM images reflecting the topographic and work function contrast can be obtained with light from an Hg lamp ($h\nu$ = 4.89 eV), which acts as a linear photoelectron excitation source.

LONGITUDINAL SURFACE PLASMON POLARITON IMAGING

As a prelude to imaging of the transverse plasmon modes, we first describe the more familiar PEEM interference imaging of the propagating longitudinal SPP modes. We confine "longitudinal" to mean that the in-plane k-vector component of the laser light (k_L) of the TM mode is parallel to the long axis of a nanowire sample. In this geometry, the external field excites an SPP mode of the Ag/vacuum interface on encountering the near edge of a wire and has a component that is parallel to the SPP propagation k-vector, k_{SPP} (Figure 1a). As the external field and the SPP wave propagate along the Ag nanowire surface with different k-vectors,[39,40] their fields add coherently to create a spatial and temporal interference pattern with a stationary envelope that is given by the difference of the inverse of k-vectors of the two fields; the interference pattern is detected with PEEM as a real-space modulation of the nonlinear mPP signal. The PEEM image in Figure 1a, therefore, represents a nonlinear map of the SPP and external field interference seen as strong modulation of the photoelectron yield emanating from the top of a Ag wire. Because the k_L of the incident field is defined precisely by the experimental geometry, the k_{SPP} of the SPP propagation can be determined. The beat period of the periodically modulated photoemission signal (λ_B) can be calculated as follows:[38]

$$\lambda_B = \frac{\lambda_L \lambda_{SPP}}{\sqrt{\lambda_L^2 + \lambda_{SPP}^2 - 2\lambda_L \lambda_{SPP} \cos(\gamma)}} \quad (1)$$

where γ denotes the angle between the k_L and the k_{SPP} (γ = 0 for the geometry in Figure 1a; $k_{SPP} = 2\pi/\lambda_{SPP}$; and $k_L = 2\pi/\lambda_L$). By recording the interference period λ_B for different excitation wavelengths, we determine a dispersion relation for the photon energy vs k_{SPP} over a wide energy range, as shown in Figure 1b. These results show the spectroscopic advantage of our broadly tunable excitation over the previous monochromatic interference imaging experiments.[20] Figure 1b aggregates the results for three different lengths of wires, L = 3.1, 5.7, and 20 μm, which are mutually consistent and in fair agreement with the dispersion of Ag bulk/vacuum interface. The small deviation from the vacuum/Ag interface dispersion relation for larger k_{SPP} is characteristic for wires and thus can be attributed to their reduced dimensionality.[32,41] Further details of the photon energy dependent longitudinal imaging will be presented elsewhere.

We note that Figure 1a shows weak modulations on the Ag monolayer covered Si(001) surface. These waves are caused by the diffraction of the incident light at the Ag nanostructures.[43] Although an acoustic plasmon mode is known for the metallic surface state band of Si(111)-($\sqrt{3} \times \sqrt{3}$)-Ag with linear dispersion reaching up to 800 meV in the high k-vector limit,[44] a plasmon mode for the semiconducting Si(001)- Ag-(2 × 3) wetting layer is not expected.[45]

TRANSVERSE SURFACE PLASMON POLARITON IMAGING

The longitudinal excitation of SPPs in metallic nanowires is intuitive and widely investigated.[6−8,33,40,46] Launching and imaging of SPPs in nanowires with other optical excitation geometries is relatively unexplored, however. Here we focus on the transverse imaging keeping in mind the lessons from the longitudinal imaging. The efficiency of coupling into the SPP modes is usually smaller for the transverse geometries than for the longitudinal one because it results from additional scattering by the structure walls.[12] We estimate that in the

DOI: 10.1021/acsphotonics.6b00353
ACS Photonics XXXX, XXX, XXX−XXX

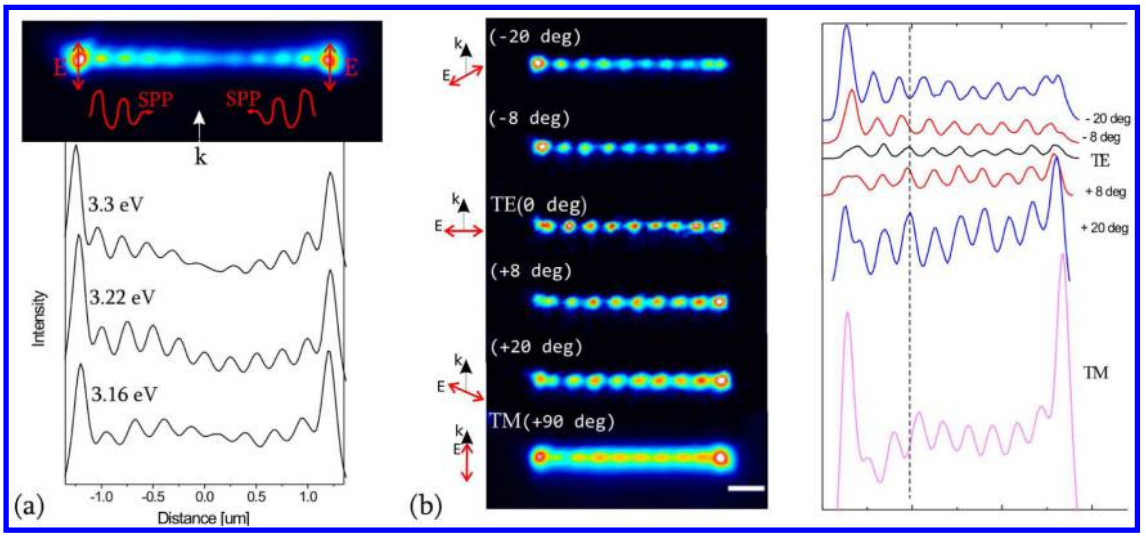

Figure 3. (a) Line profiles along a 2.5 μm long Ag wire for TM polarization with different excitation energies. At the top, a PEEM image taken at 3.3 eV is shown together with schematics of how SPPs are launched at the wire's ends. (b) Polarization rotation dependence of the plasmonic mode distribution for the same wire as in (a), measured at 3.1 eV. The rotation of the polarization is given in brackets (TM is at $\pm 90°$). The intensity of the images and line profiles for the TE mode and the nearby angles is enhanced for better visibility.

2.2−3.0 eV excitation range the maximum signal strengths are approximately 2 times stronger for the longitudinal relative to the transverse TM excitation based on a comparison with the photoemission strength from the Si(001)-Ag-(2 × 3) wetting layer. For the longitudinal excitation, the charge induced by the external field piles up at the wire ends, driving the induced dipoles to considerable strengths. Photon−plasmon coupling efficiency and damping length can change significantly for different directions of the excitation polarization, in particular for wires with a diameter of around 100 nm or larger.[12,40] Ag wires presented here have nontrivial topography,[47] with a characteristic pyramidal shape. An advantage of the LEEM/PEEM instrument is that we can characterize the crystalline and geometrical structures of *in situ* grown nanoparticles during and after the growth using the LEEM mode. According to the LEEM image in Figure 2a, the nanowire imaged in Figure 2b has an elongated, truncated pyramid structure defined by widths at the base (Ag/Si interface) of h_1 = 200 nm and at the pedestal (Ag/vacuum interface) of h_2 = 50 nm. On the basis of atomic force microscopy (AFM) measurements, the thickness of the wire is estimated to be d = 70 nm, which corresponds to 47° inclination of the pyramid side walls with respect to the surface plane, in agreement with previous reports.[48] Plasmonic wires with such dimensions, well-defined single-crystalline structure, and precisely formed interfaces are well suited for studying the effects of wavelength, polarization, and excitation geometry on excitation of various surface plasmon modes.

Representative PEEM images obtained in the transverse geometry with the laser light k_L perpendicular to the long axis of the wire for TM and TE polarizations are shown in Figure 2b. Resonant modes with periodic modulation patterns of photoemission intensity along the wire can be clearly excited for both polarizations. As $h\nu$ energy is increased, the number of evenly spaced intensity maxima increases for both polarizations. The k_{SPP} vectors for the TM (TE) excitation are extracted by assuming that intervals between the antinodes (nodes) of the modulations from experimental line profiles taken along the wire long axis correspond to λ_{SPP} (see Figure 2b). The observed series of modes in Figure 2 correspond to high-order multipoles with the fundamental dipole response expected to appear at around 0.25 eV, assuming the approximation for the resonant wavelength of the dipole as[3,46] $\lambda = 2L = 5$ μm. The observed k-vectors for a range of excitation energies are summarized in Figure 2c along with the light line in the vacuum and SPP dispersion for the bulk Ag/vacuum interface. The number on the right side of the experimental data points gives the number of antinodes (nodes) contained within the 2.5 μm long wire for the TM (TE) mode. Note that in this analysis we do not consider the beating pattern to arise from interference of plasmonic modes with the external fields. The k_{SPP} values obtained in our experiment are shifted substantially toward larger wavenumbers with respect to the Ag bulk dispersion. The reason for that is twofold. First, the dispersion relation assumed for a bulk Ag/vacuum describes the longitudinal excitation of a surface plasmon (as in Figure 1), while k_{SPP} values measured here correspond to high-order surface plasmon modes excited in the transverse geometry. Second, the dispersion relation of nanowires depends on their width as in the longitudinal excitation. On the basis of theoretical consideration for dipolar resonances in metallic wires, we expect the resonant k-vector of the plasmon mode to increase with decreasing of the wire diameter.[5,46] Therefore, it is not surprising that in the case of narrow Ag wires (with diameter $r \leq 100$ nm)[6,8] the k_{SPP}-vectors are nearly twice as large the ones measured here. Fair comparison of the plasmonic excitations in crystalline Ag wires with similar dimensions can be made with the work of Kang et al.:[49] for 440 nm excitation the spacing between the lobes obtained in their experiment[49] and here is λ_{SPP} = 300 and 311 nm, respectively. By changing the incident angle of the excitation and by analyzing the polarization of the near-field pattern with respect to the wire geometry, Kang et al.[49] also concluded that the observed modulations originate from surface plasmon resonances.

Our tunable excitation laser allows us to examine in more detail how the observed images form. A close inspection of line profile intensities for the TM excitation at three adjacent energies, $h\nu$ = 3.30, 3.22, and 3.16 eV shown in Figure 3a, leads us to conclude that, apart from localized multipolar modes, SPP wave packets are launched from opposite wire ends and propagate toward the middle, where they meet and interfere.

DOI: 10.1021/acsphotonics.6b00353
ACS Photonics XXXX, XXX, XXX−XXX

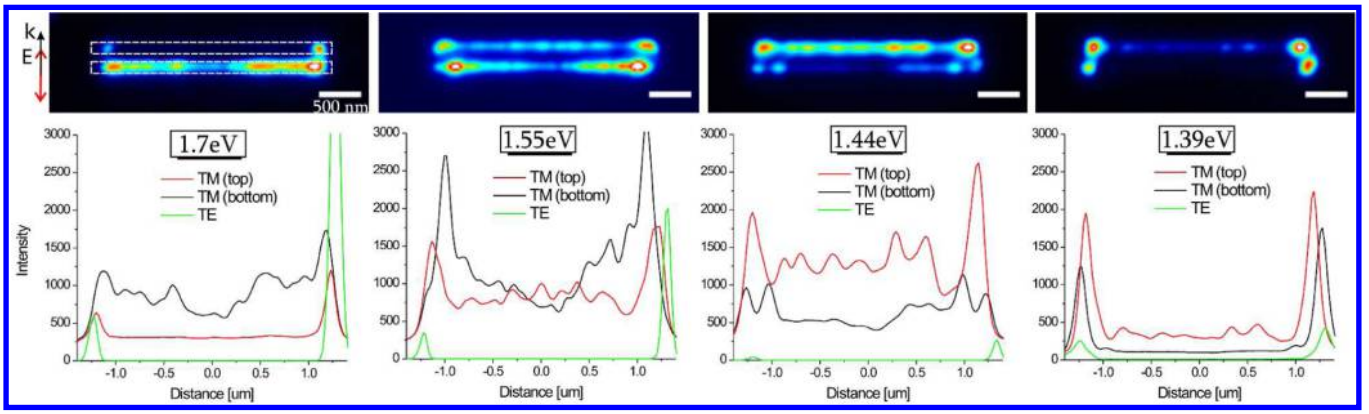

Figure 4. PEEM images for TM polarization and corresponding line profiles along the wire for TM and TE polarizations as a function of excitation energy. The line profiles are taken in the middle of the wire for TE (no splitting observed) and separately at the *top* and *bottom* for TM, to display the intensity profiles of two split modes. The Ag wire geometry is the same as in Figure 2.

These SPP wave packets can be generated only at the wire ends due to momentum conservation limitations. The intensity of the wave packets decreases toward the wire center due to the fast plasmon dephasing and therefore short propagating lengths in the UV region. The modulation amplitude is also affected by the constructive (3.22 eV) and destructive (3.30 and 3.16 eV) interferences that are evident in the wire center, where the counterpropagating waves have approximately the same amplitude and excitation wavelength dependent relative phase. Hence, the PEEM modulations observed in the transverse geometry consist of two contributions: localized multipolar modes and propagating SPPs.

Another interesting observation is the π-phase shift between the TM and TE excited oscillatory patterns. As shown in Figure 3b, rotating the polarization vector of the excitation light continuously shifts the phase of the modulations between the TM and TE limits. For TM polarization there is always one more intensity maximum in the line profiles than for the TE polarization. Moreover, the terminal TM maxima are substantially enhanced with respect to the medial maxima, whereas for the TE polarization the medial maxima are equally intense and the terminal maxima appear to be suppressed. In Figure 3b we show a progression of how the modulation patterns evolve while changing electric field direction with respect to the long axis of the wire. We observe that already for +8° (−8°) rotation from TE polarization, the right (left) terminal peak rises and forces the medial peaks to oscillate with the same phase, whereas at the left (right) end a weaker terminal peak has a phase shift with respect to the medial peaks, causing a characteristic doubled peak structure. With directions defined as in Figure 3b, a clockwise rotation of the polarization results in the phase shift toward the right end, whereas a counterclockwise rotation causes a shift toward the left. This demonstrates that the measured images reflect a shift of the surface charge distribution in the direction along the wire that is driven by the two field components. As shown by Zhang et al.[40] and Li et al.,[12] the phase of the charge distribution is related to the phase of the incident wave. Because the change of polarization of the incident wave from the TE to TM corresponds to a phase shift of π, it naturally translates into the phase shift by π of the charge distribution and, therefore, the transposition of the nodes and antinodes.

PLASMON RESONANCES AT THE Ag/Si INTERFACE

As Figure 2 demonstrates, the plasmonic response of nanowires strongly depends on the excitation photon energy. With further decrease of the energy below 1.8 eV, one would expect to observe the excitation of the lower order modes that are mandated by the dispersion behavior in Figure 2c. Instead, within the range $h\nu$ = 1.4−1.8 eV, we find that the plasmonic response of Ag nanowires deviates from the trend in Figure 2 and the PEEM images are dominated by a different class of modes with distinct spatial distributions. Representative PEEM images together with their line profiles are shown in Figure 4. Two new characteristics are observed with TM-polarized excitation: the PEEM signal splits into *top* and *bottom* branches with respect to the wire axis, and short-period oscillations appear within each branch parallel to the wire axis. We attribute these split plasmon images to high-order multipolar surface plasmon modes of the Ag/Si interface. Because the dielectric function of Si is larger than that of the vacuum, the Ag/Si interface plasmons appear at a lower energy than the surface plasmon of Ag. Similar plasmon modes have been observed by electron energy loss spectroscopy (EELS) for Ag films on Si in the 1.3−1.7 eV range[45,50,51] and have also been predicted to mediate light tunneling through nanostructured Ag/Si films.[52] Thus, considering their spatial distributions and resonant energies, we attribute the split modes to the Ag/Si interface. For the TE excitation (see line profiles in Figure 4), no modulations are present and only localized plasmons at the wire ends are excited. Similar modes are also excited with the longitudinal excitation, but only by the TE polarization. Thus, the excitation of the Ag/Si interface modes appears to be a general feature below $h\nu$ = 1.8 eV when the incident field has an in-plane component normal to the Ag nanowire axis.

As can be seen in Figure 4, changing the excitation energy modulates alternately the intensities of the *top* and *bottom* branches, which indicates that either the resonant energies are slightly different for these two regions of the wire or their coupling with the external field is different. This can be explained by recalling the fact that for the wire dimensions comparable with the excitation wavelength, and with asymmetrical (with respect to the *top* and *bottom* branches) geometry of the excitation (70° off the surface normal), retardation effects are expected to significantly affect the plasmonic mode excitation and, therefore, the observed PEEM

DOI: 10.1021/acsphotonics.6b00353
ACS Photonics XXXX, XXX, XXX−XXX

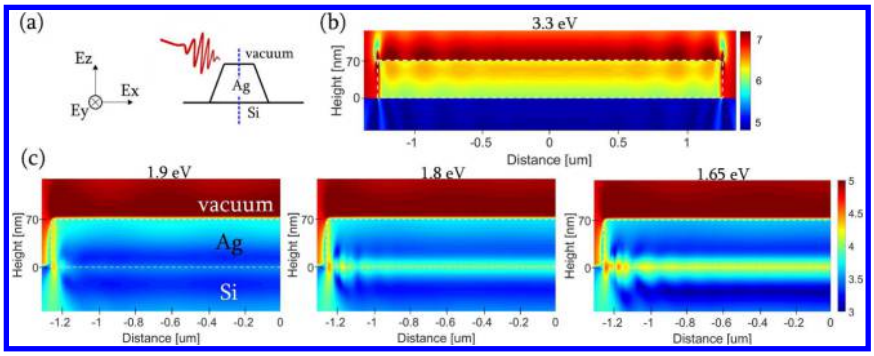

Figure 5. (a) Geometry for the FDTD simulations. The field amplitudes are calculated for the YZ cross section cutting through the middle of the Ag wire at the position of the dashed blue line. (b) Time-integrated distribution of the $|E_z|$ component obtained for $h\nu$ = 3.3 eV. (c) Time-integrated $|E_z|$ component for varying excitation energy showing the onset of plasmonic resonances at the Ag/Si interface. Note that different scales for z and x,y axes are used for better visibility of the interfaces. The color scales are logarithmic.

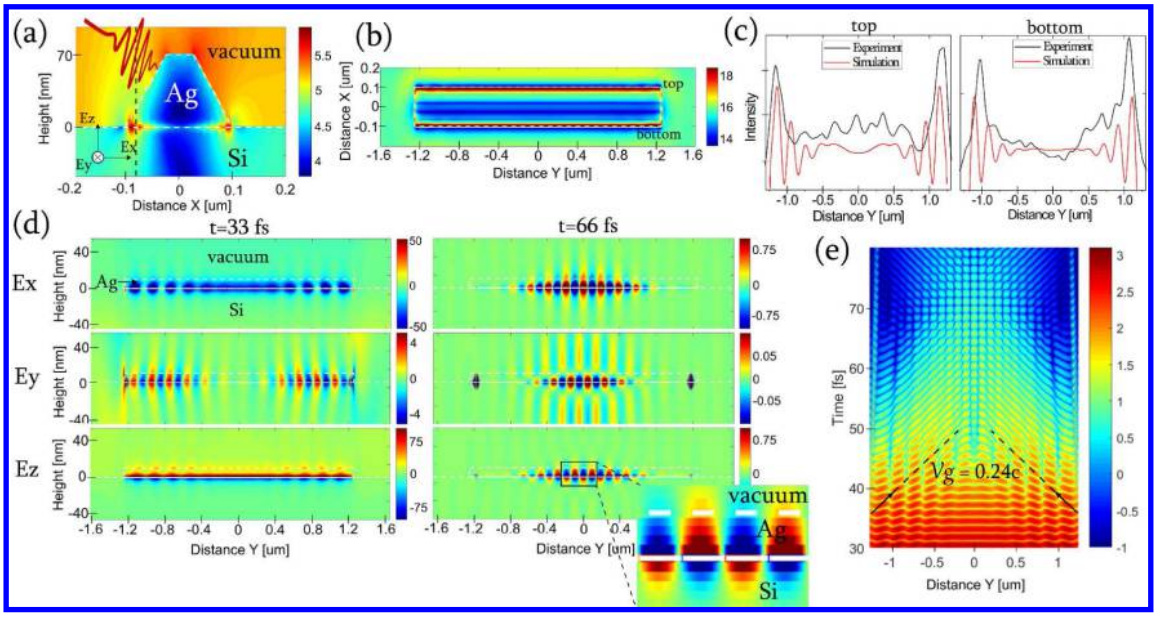

Figure 6. FDTD simulations of E-fields excited on a Ag nanowire on Si for TM excitation with 800 nm ($h\nu$ = 1.55 eV) light. The wire dimensions are as defined in Figure 2a. (a) Time-integrated total electric field intensity E_{tot} across the XZ plane in the middle of the Ag wire. (b) Simulated PEEM image in the XY plane for E_{tot} evaluated 2 nm below the Ag/vacuum and Si/vacuum interfaces. (c) Line profiles taken from the simulated PEEM image in (b) along "top" and "bottom" edges of the wire. For comparison, line profiles from the experimental PEEM images in Figure 4 are plotted. (d) Snapshots of the electric field components E_x, E_y, and E_z at the YZ plane, 10 nm away from the front edge, as indicated by the black dashed line in (a). The enlarged area in the inset illustrates the phase shift between the Si and Ag regions for the E_z component. (e) Time evolution of the $|E_z|$ component integrated over 4 nm around the Ag/Si interface. Note that different scales for z and x,y axes are used for better visibility of the interfaces. (a), (b), (c), and (e) are in a logarithmic scale, while (d) is in a linear color scale.

signal. In addition, even small deviations in the wire geometry can result in different lengths of the *top* and *bottom* branches and, hence, affect their resonances. By changing the photon energy we can selectively excite the *bottom* ($h\nu$ = 1.7 eV) or the *top* ($h\nu$ = 1.44 and 1.39 eV) wire edges. At $h\nu$ = 1.55 eV, the *bottom* and the *top* branches resonate simultaneously, with averaged periods (excluding the edge peaks) of the modulations λ_{SPP} = 195 and 225 nm (±15 nm), respectively.

NUMERICAL SIMULATIONS AND DISCUSSION

On the basis of our experimental findings we report two types of plasmon resonances in the transverse geometry: (i) pedestal plasmons at the Ag/vacuum interface (Figures 2 and 3), which dominate for $h\nu \geq 1.9$ eV; and (ii) Ag/Si interface plasmons at the wire base (Figures 4), which dominate for $h\nu \leq 1.8$ eV. To obtain further insight into the various plasmonic modes of Ag nanowires, we present finite-difference time-domain (FDTD) simulations of electromagnetic fields excited within Si-supported Ag nanowires, from which we can extract the E_x, E_y, and E_z components of electric fields at different wire cross sections for excitation with various incident polarizations and excitation energies. Ag wire with dimensions comparable to the experimental one in Figure 2a is simulated by a total field scattered field source assuming a pulse duration of 30 fs. The simulation duration is 300 fs.

In Figure 5 we present time-integrated distribution of the $|E_z|$ component at the wire cross section along the YZ plane (marked by the dashed blue line in Figure 5a), obtained with different excitation energies for TM-polarized transverse excitation. Although the mechanism of plasmon excitation and its time evolution are similar for all three components, the simulations show that the E_y makes negligible contribution to the total field, except at the wire ends, being one order of

DOI: 10.1021/acsphotonics.6b00353
ACS Photonics XXXX, XXX, XXX−XXX

magnitude smaller than the E_x and E_z amplitudes. E_y is small because the external field has no component in the y direction, and therefore it is purely of surface plasmon origin. At $h\nu$ = 3.3 eV (λ = 376 nm; Figure 5b), the calculated $|E_z|$ amplitude modulations are visible at the Ag/vacuum interface; their period, determined by the E_x and E_z intensities, is constant along the wire and equal to λ_{SPP} = 260 nm. This value is in good agreement with our experimental period λ_{SPP} = 234 nm. We note that there are no indications of resonances at the Ag/Si interface at this excitation energy.

Next we examine the $|E_z|$ component as a function of the excitation wavelength in Figure 5c. We find that the Ag/Si plasmons start to appear at $h\nu$ = 1.8 eV (λ = 690 nm) and are clearly present upon decreasing the excitation energy to $h\nu$ = 1.65 eV. The energy threshold of $h\nu \leq$ 1.8 eV for the Ag/Si resonance obtained from the simulations corresponds exactly to the energy at which splitting of the wire into two branches appears in the PEEM images. Note however that the Ag/Si interface cannot be observed at the YZ plane (blue dashed line in Figure 5a) in the PEEM images because the electron escape depth (<5 nm) is much smaller than the 70 nm pyramid height. The signal attributed to the internal interface can be observed experimentally only by photoemission from the selvedge region where the Ag pyramid sides terminate in the atomically sharp Ag-(2 × 3) wetting layer on Si terraces. This naturally leads to splitting of the PEEM signal into two branches, as observed in Figure 4, and corresponds to the enhanced photoemission from the selvedge regions.

To grasp the distribution of the Ag/Si interface plasmon in three dimensions and its correspondence to the PEEM images, other cross sections from the FDTD simulations are presented in Figure 6. The time-integrated total electric field $E_{tot} = \sqrt{E_x^2 + E_y^2 + E_z^2}$ is shown in Figure 6a for the wire cross section in the XZ plane. Strong enhancement of the electric field at the wire base corners can be attributed to the atomically sharp base vertices. Thus, the observation of Ag/Si interface plasmons can be attributed both to the existence of such modes for $h\nu \leq$ 1.8 eV and to their enhancement at the Ag/Si selvedge. To make a direct comparison with the experimental PEEM images, the PEEM intensity, I_{PEEM}, from the simulation is calculated by

$$I_{PEEM} = \int_0^T (E_{tot}(x, y, t))^{2n}\, dt \qquad (2)$$

where T designates the time for the coherent fields to die out, which for the purpose of the simulation equals 300 fs, and n is the photoemission order corresponding to the number of photons required to excite electrons above the vacuum barrier.[39] E_{tot} includes both the excitation and the internal plasmon fields. In Figure 6b, the simulated PEEM image for a 3PP process (n = 3) with $h\nu$ = 1.55 eV is shown. As the polarization occurs within the material, the plane for evaluating the PEEM intensity is defined by following the geometry of the wire and evaluating the fields exactly 2 nm below the Ag/vacuum and Si/vacuum interfaces. The white dashed line defines the edges of the wire base. The strongest enhancement of the PEEM signal is observed at the Ag/Si edges, in agreement with the experiment (see PEEM image at 1.55 eV in Figure 4). Due to high localization of the fields at the bottom apexes of the Ag wire, the periodicity of the modulations is hardly noticeable just by looking at the PEEM image. The line profiles taken along the *top* and *bottom* edges are plotted together with the experimental line profiles in (c). The averaged period of the modulations in the simulation (excluding the edge peaks and the beating long period in the center) equals λ_{SPP} = 202 and 204 nm (±5 nm) at the *bottom* and the *top* edge, respectively, in good agreement with the corresponding experimental values of λ_{SPP} = 195 and 225 nm (±15 nm). In addition, in both the experiment and simulation, the amplitude of the modulations decreases toward the middle of the wire. In fact, in particular in the simulation, the oscillatory behavior along the edges is nearly entirely suppressed in the middle of the wire (y = 0). One has to realize, however, that integrating over time averages some of the oscillations of the excited fields.

To understand the origins of the calculated modulations in the time-integrated signal, it is valuable to analyze the time evolution of the electric field distribution. In Figure 6d, the E_x, E_y, and E_z components for $h\nu$ = 1.55 eV are shown for two time frames, t = 33 and 66 fs (t = 0 fs corresponds to the maximum amplitude of the external field passing through the structure). To access the Ag/Si plasmons localized at the wire edges, the cross sections along the wire are taken at the YZ plane, 10 nm away from the wire base edge, as indicated by the black dashed line in Figure 6a. This plane corresponds to the cross section of the *bottom* edge. Upon excitation with a laser light, multipolar modes are excited at the Ag/Si interface with the period of the modulations equal to λ_{SPP} = 194 nm. The amplitude of the oscillations is the largest at the wire ends and decreases toward the center of the long axis of the wire. All three components travel toward the center of the wire with a group velocity $V_g = \partial\omega/\partial k$. By tracing the displacement of peak maxima as a function of time, we obtain the group velocity V_g = 0.24c (where c is the speed of light in a vacuum) of the E_{tot} wave packet in the direction along the long axis of the wire. To visualize how the SPPs move in space and time, time evolution of the E_z component integrated over a 4 nm area around the Ag/Si interface is plotted in Figure 6e. The peak maxima move toward the center of the wire with a velocity V_g = 0.24c defined by the slope V_g = distance/time (as marked by the black dashed lines in Figure 6e). Because with every optical cycle (2.67 fs at this wavelength) the multipolar modes are excited at the same positions of the wire, there is no movement of the peaks in a time-integrated picture. Only when the external driving field is of negligible strength (longer than ∼50 fs) can the counter-propagating peak maxima be seen to travel freely along the wire and eventually overlap at ∼70 fs, resulting in an enhanced amplitude in the middle of the wire. Such interference of SPP wave packets can explain the long/beating period, superimposed on the short-period modulations (see line profiles in Figure 4 and Figure 6c).

In the case of Ag/vacuum plasmons, time evolution of the field components as seen in the FDTD simulations is qualitatively similar; that is, the peaks are observed to travel toward the center of the wire and interfere only after the external driving field has decayed to a negligible strength. In the case of the Ag/vacuum interface, however, the wave packets excited with $h\nu$ =1.55 eV travel with a speed V_g = 0.5c, i.e., roughly 2 times faster than the ones at the Ag/Si interface. One should note that effective velocities V_g of the total signals E_{tot} contain multiple contributions from scattered fields and internal plasmon fields and cannot be unambiguously interpreted as the surface plasmon group velocities.

Another property, which is particular to the Ag/Si plasmon mode, is the symmetry with respect to the interface. It is well

DOI: 10.1021/acsphotonics.6b00353
ACS Photonics XXXX, XXX, XXX−XXX

established that thin metallic structures below 100 nm support coupled modes of the dielectric−metal film−dielectric structure.[53,54] When the top and bottom dielectrics are identical, these are rigorously antisymmetric a_b and symmetric s_b bound modes, with the s_b fields predominantly existing in the dielectric and the a_b mode in the metal. The symmetry of the bound mode is defined with respect to the transverse, i.e., perpendicular to the interface electric field distribution.[53,54] As the metal film thickness is reduced, the s_b mode experiences weaker interaction with the metal film and consequently is named the *long-range* plasmon, whereas the a_b mode experiences stronger confinement, and therefore faster damping, and thus is known as the *short-range* surface plasmon.[55] In the case of Ag nanowires on a Si substrate, the dielectric structure is not symmetric because bottom and top dielectrics are made of different materials, and the Ag film thickness varies continuously in the selvedge region. Because Si is a high-index material relative to a vacuum, substantial deviations from the symmetric structure model are expected.[56] We see in the inset of Figure 6d that the E_z component is odd with respect to the vacuum/Ag/Si interface; that is, it undergoes a sign (phase) change, whereas the E_x, E_y components are even. This behavior is expected for the antisymmetric a_b mode of the vacuum/Ag/Si construct. Because the skin depth of Ag for the visible light is in the range of 20 nm, the effect of coupling between the plasmonic fields from the bottom Ag/Si and the top Ag/vacuum interfaces is of negligible strength at the pedestal of our 70 nm thick Ag wire.

CONCLUSIONS

In summary, we performed a spectromicroscopic study of the plasmonic resonances excited in epitaxial Ag nanowires on a Si(001) substrate. Our results show that Ag wires with dimensions comparable to the excitation wavelength and characteristic pyramidal shape are very versatile plasmonic systems possessing both propagating and multipolar surface plasmons, which can be selectively excited depending on the excitation geometry and light polarization. In particular, we demonstrated the excitation of the transverse higher order surface plasmon modes driven by the incident laser light with *k*-vector perpendicular to the major axis of the wire. By tuning the energy of the excitation laser light we distinguish two types of bound modes, localized at the Ag/vacuum and the Ag/Si interfaces. Although both modes can be excited with near-IR light, the Ag/Si modes make the dominant contributions to the photoemission signals in part due to a much stronger field confinement. By combining the real-space imaging using PEEM together with FDTD simulations we explain the mechanisms of the plasmon excitation and propagation.

Previous studies on plasmonic modes in metallic nanowires have been mostly limited to the longitudinal excitations where Fabry−Perot-like interferences of the counterpropagating SPP waves were observed in the quasistatic limit.[6−9] Such interferences result in standing wave patterns with periodicity defined by $\lambda_{SPP}/2$, but they do not represent truly localized high-order modes. PEEM experiments are not very sensitive to Fabry−Perot modes, because they require time to establish through propagation, reflection, and interference of counter-propagating SPP waves and therefore are weaker than the primary interferences between the traveling waves. Nevertheless, in wavelength size structures Fabry−Perot modes can modulate the PEEM intensities.[57] Although localized high-order plasmonic modes are usually neglected in the literature due to very short propagation lengths, the results of Norrman et al.[58] show the possibility of the transition of higher order modes into dominant modes with long propagation lengths. An estimation for the existence of higher order modes, $\varepsilon_{r1} \leq \varepsilon_{r2}$, where ε_{r1} and ε_{r2} denote relative permittivity of the metallic slab and the surrounding media, respectively, is indeed fulfilled for our Ag/Si structure.

Considering that the Ag/Si plasmons exist above the indirect band gap of Si, the transfer of energy from the interface plasmons to electron−hole excitation in Si should be efficient. Thus, the Ag/Si interface plasmons are more likely to be important for plasmonically enhanced photochemistry than the Ag/vacuum plasmons, which contribute to excitation of the Si substrate mainly through scattering processes. The Ag/vacuum plasmon modes are likely to be brighter in optical scattering experiments, however, and thereby give a misleading impression of being the dominant mode of coupling external fields into semiconductor electron−hole pair excitation. The spectrally broadband characteristic of plasmonic resonances we have investigated might therefore be particularly beneficial in the area of research concerning plasmon-enhanced solar energy conversion and photocatalysis in metal/semiconductor hybrid structures.

AUTHOR INFORMATION

Corresponding Author

*E-mail: petek@pitt.edu.

Notes

The authors declare no competing financial interest.

ACKNOWLEDGMENTS

The authors thank R. Tromp and J. Garcia de Abajo for advice regarding the operation of AC-PEEM and modeling of plasmonic phenomena. We also acknowledge the help of Jeremy Levy, Gurudev Dutt, and Simulation and Modeling (SAM) Center at the University of Pittsburgh. This research was supported by NSF Grant CHE-1414466.

REFERENCES

(1) Zhang, J.; Zhang, L. Nanostructures for Surface Plasmons. *Adv. Opt. Photonics* **2012**, *4*, 157−321.

(2) Atwater, H. A.; Polman, A. Plasmonics for Improved Photovoltaic Devices. *Nat. Mater.* **2010**, *9*, 205−213.

(3) Neubrech, F.; Pucci, A.; Cornelius, T. W.; Karim, S.; Garcia-Etxarri, A.; Aizpurua, J. Resonant Plasmonic and Vibrational Coupling in a Tailored Nanoantenna for Infrared Detection. *Phys. Rev. Lett.* **2008**, *101*, 157403.

(4) Muhlschlegel, P.; Eisler, H.-J.; Martin, O. J. F.; Hecht, B.; Pohl, D. W. Resonant Optical Antennas. *Science* **2005**, *308*, 1607−1609.

(5) Bryant, G. W.; Garcia de Abajo, F. J.; Aizpurua, J. Mapping the Plasmon Resonances of Metallic Nanoantennas. *Nano Lett.* **2008**, *8*, 631−636.

(6) Ditlbacher, H.; Hohenau, A.; Wagner, D.; Kreibig, U.; Rogers, M.; Hofer, F.; Aussenegg, F. R.; Krenn, J. R. Silver Nanowires as Surface Plasmon Resonators. *Phys. Rev. Lett.* **2005**, *95*, 257403.

(7) Dorfmuller, J.; Vogelgesang, R.; Weitz, R. T.; Rockstuhl, C.; Etrich, C.; Pertsch, T.; Lederer, F.; Kern, K. Fabry-Perot Resonances in One-Dimensional Plasmonic Nanostructures. *Nano Lett.* **2009**, *9*, 2372−2377.

(8) Rossouw, D.; Couillard, M.; Vickery, J.; Kumacheva, E.; Botton, G. A. Multipolar Plasmonic Resonances in Silver Nanowire Antennas Imaged with a Subnanometer Electron Probe. *Nano Lett.* **2011**, *11*, 1499−1504.

(9) Piazza, L.; Lummen, T.; Quinonez, E.; Murooka, Y.; Reed, B.; Barwick, B.; Carbone, F. Simultaneous Observation of the

DOI: 10.1021/acsphotonics.6b00353
ACS Photonics XXXX, XXX, XXX−XXX

Quantization and the Interference Pattern of a Plasmonic Near-Field. *Nat. Commun.* **2015**, *6*, 6407.
(10) Lee, H. S.; Kim, M. S.; Jin, Y.; Han, G. H.; Lee, Y. H.; Kim, J. Efficient Exciton-Plasmon Conversion in Ag Nanowire/Monolayer MoS_2 Hybrids: Direct Imaging and Quantitative Estimation of Plasmon Coupling and Propagation. *Adv. Opt. Mater.* **2015**, *3*, 943−947.
(11) Dong, J.; Wang, J.; Ma, F.; Cheng, Y.; Zhang, H.; Zhang, Z. Recent Progresses in Integrated Nanoplasmonic Devices Based on Propagating Surface Plasmon Polaritons. *Plasmonics* **2015**, *10*, 1841−1852.
(12) Li, Z.; Bao, K.; Fang, Y.; Huang, Y.; Nordlander, P.; Xu, H. Correlation between Incident and Emission Polarization in Nanowire Surface Plasmon Waveguides. *Nano Lett.* **2010**, *10*, 1831−1835.
(13) Clavero, C. Plasmon-Induced Hot-Electron Generation at Nanoparticle/Metal-Oxide Interfaces for Photovoltaic and Photocatalytic Devices. *Nat. Photonics* **2014**, *8*, 95−103.
(14) Catchpole, K.; Polman, A. Plasmonic Solar Cells. *Opt. Express* **2008**, *16*, 21793−21800.
(15) Li, J.; Cushing, S. K.; Meng, F.; Senty, T. R.; Bristow, A. D.; Wu, N. Plasmon-Induced Resonance Energy Transfer for Solar Energy Conversion. *Nat. Photonics* **2015**, *9*, 601−607.
(16) Polman, A.; Atwater, H. A. Photonic Design Principles for Ultrahigh-Efficiency Photovoltaics. *Nat. Mater.* **2012**, *11*, 174−177.
(17) Li, G.; Cherqui, C.; Bigelow, N. W.; Duscher, G.; Straney, P. J.; Millstone, J. E.; Masiello, D. J.; Camden, J. P. Spatially Mapping Energy Transfer from Single Plasmonic Particles to Semiconductor Substrates via STEM/EELS. *Nano Lett.* **2015**, *15*, 3465−3471.
(18) Wu, K.; Chen, J.; McBride, J. R.; Lian, T. Efficient Hot-Electron Transfer by a Plasmon-Induced Interfacial Charge-Transfer Transition. *Science* **2015**, *349*, 632−635.
(19) Goodfellow, K. M.; Beams, R.; Chakraborty, C.; Novotny, L.; Vamivakas, A. N. Integrated Nanophotonics Based on Nanowire Plasmons and Atomically Thin Material. *Optica* **2014**, *1*, 149−152.
(20) Chelaru, L. I.; zu Heringdorf, F.-J. M. In Situ Monitoring of Surface Plasmons in Single-Crystalline Ag-Nanowires. *Surf. Sci.* **2007**, *601*, 4541−4545.
(21) Enoch, S.; Bonod, N. *Plasmonics: From Basics to Advanced Topics*; Springer: Berlin Heidelberg, 2012; p 167.
(22) Kubo, A.; Onda, K.; Petek, H.; Sun, Z.; Jung, Y. S.; Kim, H. K. Femtosecond Imaging of Surface Plasmon Dynamics in a Nanostructured Silver Film. *Nano Lett.* **2005**, *5*, 1123−1127.
(23) Kravtsov, V.; Ulbricht, R.; Atkin, J. M.; Raschke, M. B. Plasmonic Nanofocused Four-Wave Mixing for Femtosecond Near-Field Imaging. *Nat. Nanotechnol.* **2016**, *11*, 459−464.
(24) Petek, H. Imaging: Nano Meets Femto. *Nat. Nanotechnol.* **2016**, *11*, 404−405.
(25) Petek, H. Single-Molecule Femtochemistry: Molecular Imaging at the Space-Time Limit. *ACS Nano* **2014**, *8*, 5−13.
(26) Garcia de Abajo, F. J. Optical Excitations in Electron Microscopy. *Rev. Mod. Phys.* **2010**, *82*, 209−275.
(27) Feist, A.; Echternkamp, K. E.; Schauss, J.; Yalunin, S. V.; Schafer, S.; Ropers, C. Quantum Coherent Optical Phase Modulation in an Ultrafast Transmission Electron Microscope. *Nature* **2015**, *521*, 200−203.
(28) Aeschlimann, M.; Brixner, T.; Fischer, A.; Kramer, C.; Melchior, P.; Pfeiffer, W.; Schneider, C.; Strber, C.; Tuchscherer, P.; Voronine, D. V. Coherent Two-Dimensional Nanoscopy. *Science* **2011**, *333*, 1723−1726.
(29) Fujikawa, Y.; Sakurai, T.; Tromp, R. M. Surface Plasmon Microscopy Using an Energy-Filtered Low Energy Electron Microscope. *Phys. Rev. Lett.* **2008**, *100*, 126803.
(30) Kawano, H. Effective Work Functions for Ionic and Electronic Emissions from Mono- and Polycrystalline Surfaces. *Prog. Surf. Sci.* **2008**, *83*, 1−165.
(31) Cinchetti, M.; Gloskovskii, A.; Nepjiko, S. A.; Schönhense, G.; Rochholz, H.; Kreiter, M. Photoemission Electron Microscopy as a Tool for the Investigation of Optical Near Fields. *Phys. Rev. Lett.* **2005**, *95*, 047601.
(32) Schider, G.; Krenn, J. R.; Hohenau, A.; Ditlbacher, H.; Leitner, A.; Aussenegg, F. R.; Schaich, W. L.; Puscasu, I.; Monacelli, B.; Boreman, G. Plasmon Dispersion Relation of Au and Ag Nanowires. *Phys. Rev. B: Condens. Matter Mater. Phys.* **2003**, *68*, 155427.
(33) Taminiau, T. H.; Stefani, F. D.; van Hulst, N. F. Optical Nanorod Antennas Modeled as Cavities for Dipolar Emitters: Evolution of Sub- and Super-Radiant Modes. *Nano Lett.* **2011**, *11*, 1020−1024.
(34) Tromp, R.; Hannon, J.; Ellis, A.; Wan, W.; Berghaus, A.; Schaff, O. A New Aberration-Corrected, Energy-Filtered LEEM/PEEM Instrument. I. Principles and Design. *Ultramicroscopy* **2010**, *110*, 852−861.
(35) Mundschau, M.; Bauer, E.; Telieps, W.; Swiech, W. Atomic Steps on Si(100) and Step Dynamics During Sublimation Studied by Low-Energy Electron Microscopy. *Surf. Sci.* **1989**, *223*, 413−423.
(36) Roos, K. R.; Roos, K. L.; von Hoegen, M. H.; zu Heringdorf, F.-J. M. High Temperature Self-Assembly of Ag Nanowires on Vicinal Si(001). *J. Phys.: Condens. Matter* **2005**, *17*, S1407.
(37) Wall, D.; Sindermann, S.; Roos, K. R.; von Hoegen, M. H.; zu Heringdorf, F.-J. M. The Influence of Anisotropic Diffusion on Ag Nanowire Formation. *J. Phys.: Condens. Matter* **2009**, *21*, 314023.
(38) Kubo, A.; Jung, Y. S.; Kim, H. K.; Petek, H. Femtosecond Microscopy of Localized and Propagating Surface Plasmons in Silver Gratings. *J. Phys. B: At., Mol. Opt. Phys.* **2007**, *40*, S259−S272.
(39) Kubo, A.; Pontius, N.; Petek, H. Femtosecond Microscopy of Surface Plasmon Polariton Wave Packet Evolution at the Silver/Vacuum Interface. *Nano Lett.* **2007**, *7*, 470−475.
(40) Zhang, L.; Kubo, A.; Wang, L.; Petek, H.; Seideman, T. Imaging of Surface Plasmon Polariton Fields Excited at a Nanometer-Scale Slit. *Phys. Rev. B: Condens. Matter Mater. Phys.* **2011**, *84*, 245442.
(41) Schmidt, F.-P.; Ditlbacher, H.; Hohenester, U.; Hohenau, A.; Hofer, F.; Krenn, J. R. Universal Dispersion of Surface Plasmons in Flat Nanostructures. *Nat. Commun.* **2014**, *5*, 3604.
(42) Johnson, P. B.; Christy, R. W. Optical Constants of the Noble Metals. *Phys. Rev. B* **1972**, *6*, 4370−4379.
(43) Chelaru, L. I.; von Hoegen, M. H.; Thien, D.; zu Heringdorf, F.-J. M. Fringe Fields in Nonlinear Photoemission Microscopy. *Phys. Rev. B: Condens. Matter Mater. Phys.* **2006**, *73*, 115416.
(44) Nagao, T.; Hildebrandt, T.; Henzler, M.; Hasegawa, S. Dispersion and Damping of a Two-Dimensional Plasmon in a Metallic Surface-State Band. *Phys. Rev. Lett.* **2001**, *86*, 5747.
(45) Kim, S.-K.; Kim, J.-S.; Lee, G.; Nogami, J.; Kong, K.-j.; Yu, B.; Ahn, D. Electronic Structure of p(2 × 3) Ag Films on Si(100). *J. Korean Phys. Soc.* **2013**, *2*, 86−91.
(46) Novotny, L. Effective Wavelength Scaling for Optical Antennas. *Phys. Rev. Lett.* **2007**, *98*, 266802.
(47) Huang, Q.; Lilley, C. M.; Bode, M. Surface scattering Effect on the Electrical Resistivity of Single Crystalline Silver Nanowires Self-Assembled on Vicinal Si(001). *Appl. Phys. Lett.* **2009**, *95*, 103112.
(48) Kong, D.; Drucker, J. Tuning Ag/Si(100) Island Size, Shape, and Density. *J. Appl. Phys.* **2013**, *114*, 144310.
(49) Kang, T.; Choi, W.; Yoon, I.; Lee, H.; Seo, M.-K.; Park, Q.-H.; Kim, B. Rainbow Radiating Single-Crystal Ag Nanowire Nanoantenna. *Nano Lett.* **2012**, *12*, 2331−2336.
(50) Layet, J.; Contini, R.; Derrien, J.; Luth, H. Coupled Interface Plasmons of the Ag-Si(111) System as Investigated with High-Resolution Electron Energy-Loss Spectroscopy. *Surf. Sci.* **1986**, *168*, 142−148.
(51) Politano, A.; Chiarello, G. The Influence of Electron Confinement, Quantum Size Effects, and Film Morphology on the Dispersion and the Damping of Plasmonic Modes in Ag and Au Thin Films. *Prog. Surf. Sci.* **2015**, *90*, 144−193.
(52) Garcia de Abajo, F. J.; Gomez-Santos, G.; Blanco, L. A.; Borisov, A. G.; Shabanov, S. V. Tunneling Mechanism of Light Transmission through Metallic Films. *Phys. Rev. Lett.* **2005**, *95*, 067403.
(53) Sarid, D. Long-Range Surface-Plasma Waves on Very Thin Metal Films. *Phys. Rev. Lett.* **1981**, *47*, 1927−1930.
(54) Wang, L.-M.; Zhang, L.; Seideman, T.; Petek, H. Dynamics of Coupled Plasmon Polariton Wave Packets Excited at a Subwavelength

DOI: 10.1021/acsphotonics.6b00353
ACS Photonics XXXX, XXX, XXX−XXX

Slit in Optically Thin Metal Films. *Phys. Rev. B: Condens. Matter Mater. Phys.* **2012**, *86*, 165408.
(55) Berini, P. Long-Range Surface Plasmon Polaritons. *Adv. Opt. Photonics* **2009**, *1*, 484−588.
(56) Dionne, J. A.; Sweatlock, L. A.; Sheldon, M. T.; Alivisatos, A. P.; Atwater, H. A. Silicon-Based Plasmonics for On-Chip Photonics. *IEEE J. Sel. Top. Quantum Electron.* **2010**, *16*, 295−306.
(57) Zhang, L.; Kubo, A.; Wang, L.; Petek, H.; Seideman, T. Universal Aspects of Ultrafast Optical Pulse Scattering by a Nanoscale Asperity. *J. Phys. Chem. C* **2013**, *117*, 18648−18652.
(58) Norrman, A.; Setl, T.; Friberg, A. T. Long-Range Higher-Order Surface-Plasmon Polaritons. *Phys. Rev. A: At., Mol., Opt. Phys.* **2014**, *90*, 053849.

DOI: 10.1021/acsphotonics.6b00353
ACS Photonics XXXX, XXX, XXX−XXX